JOURNAL OF MATERIALS SCIENCE 33 (1998) 4059–4068

Micromorphology-dependent mechanical properties of syndiotactic polystyrene

S. ST LAWRENCE, D. M. SHINOZAKI*
Department of Mechanical and Materials Engineering, The University of Western Ontario, London, Ontario, Canada N6A 5B9
E-mail: shinozak@julian.uwo.ca

The crystallization history of syndiotactic polystyrene is found to affect strongly its mechanical properties. Samples cooled slowly from the melt have much higher moduli than do samples quenched from the melt (to the amorphous state) and subsequently heated to induce crystallization just above T_g. The differences are not due to differences in crystallinity. Examination of the lamellar structure and micromechanical modelling of the two different micromorphologies which evolve, show that the most likely reasons for these differences are the constraint of the amorphous phase by the high-modulus lamellae, and the variation in phase contiguity. In slowly cooled samples, the crystalline phase is contiguous (mechanically), and the interlamellar amorphous material is more highly constrained than in the quenched–annealed samples. © *1998 Kluwer Academic Publishers*

1. Introduction

Syndiotactic polystyrene (sPS) is a partially crystalline polymer which is the subject of both practical and fundamental interest [1–15]. There have been a number of studies conducted to characterize its structure and morphology following different processing conditions [2–11]. The amount of crystallinity, the crystal structure and morphology can be changed by changing the crystallization conditions. For thin sections, of the order of 0.5 mm, rapid cooling results in almost no crystallinity. For larger cross-sections, the surface region is amorphous while the centre is largely crystalline [7–9]. The properties which make sPS attractive as an engineering thermoplastic (high-temperature mechanical properties, low permeability, good chemical resistance) are strongly affected by the amount and distribution of the crystalline phase. Earlier work has shown that the crystallization processes from the melt and from the quenched amorphous state are controlled by different parameters, suggesting a significant difference in crystalline morphology, which was confirmed by transmission electron microscopy [10]. In a practical sense, industrial processing can involve crystallization from the melt or from the quenched, amorphous state. There have been relatively few published studies comparing the mechanical properties in these two cases. The dynamic mechanical properties sPS have been studied [5, 6, 12]. De Candia *et al.* have reported a substantial difference in dynamic modulus of sample crystallized at different temperatures [5], and have suggested that this may be due to variations in lamellar morphology.

The present work examines this observation in more detail and develops a micromechanical rationale which is consistent with the observed lamellar morphology.

2. Experimental procedure

Syndiotactic polystyrene ($\bar{M}_w = 3.72 \times 10^5$) was supplied in the form of pellets from Dow Chemical Canada. Plaques for the dynamic mechanical analysis were formed by melting the pellets at 340 °C for 5 min in mould. The moulded samples were either slowly cooled from the melt (labelled SC) or rapidly cooled by quenching in cold water (labelled RC) The plaques were approximately 3 mm thick, 30 mm long and 18 mm wide. Before and after the dynamic mechanical test, the crystalline content, the crystal structure and the crystalline morphology of both types of sample were characterized.

The dynamic mechanical tests were performed in a single cantilever bending configuration at a frequency of 1 Hz using a Polymer Laboratories DMTA. The temperature range included the glass transition of the amorphous phase at 100 °C, but was well below the nominal crystalline melting point at 270 °C (50 °C $< T <$ 250 °C). The tests started at the low-temperature limit and increased at a rate of 5 °C min^{-1}, linearly with respect to time, similar to the heating process in the differential scanning calorimeter. In addition to the variously prepared sPS samples (slowly cooled from the melt and quenched from the melt), atactic samples of polystyrene with similar molecular weight were tested (to a maximum of 160 °C).

Samples weighing approximately 10 mg were cut from the moulded plaques for thermal analysis. These

* Author to whom correspondence should be addressed.

samples were used to measure the crystalline content and to characterize the changes in the thermal properties which occurred during the mechanical test. The crystalline content was determined using the method proposed by Krzystowczyk *et al.* [13]. The samples were heated at a rate of $80\,^{\circ}C\,min^{-1}$ in the DSC (Perkin–Elmer DSC 7) to a temperature above the melting point. A rapid heating rate was used to minimize the recrystallization which occurs during the DSC scan [14]. The areas of the crystallization exotherm and the melting endotherm were measured and the crystallinity estimated from the relative difference, using the value for latent heat of melting suggested by Pasztor *et al.* ($\Delta H_m^0 = 53\ (J\,g^{-1})$) [15].

Sections cut from the moulded plaques were heated much more slowly to determine the glass transition temperature, (T_g), the temperature at which melting was first detected, and the temperature range over which crystallization occurred. The linear heating rate ($5\,^{\circ}C\,min^{-1}$) that was used in these DSC scans was identical to that used in the dynamical mechanical tests. The thermal histories of the DMTA tests and the DSC scans were therefore similar. For all the DSC measurements, the instrument baseline and temperature calibrations were carefully repeated to ensure reproducibility of experimental conditions.

The crystal structure of the moulded plaques was identified from wide-angle X-ray diffraction patterns taken prior to and following the mechanical test (using a Phillips diffractometer with CuK_α radiation and a nickel filter). The samples were scanned from $2\theta = 5^{\circ}$ –25° with a step size of 0.02°. The diffractometer was carefully aligned and calibrated using a permaquartz standard for each run.

The quenched samples were prepared for optical microscopy by cutting thin sections in a plane perpendicular to the specimen's long axis. The samples were sliced from the plaque using a diamond impregnated slow speed cut-off wheel, and then embedded in an epoxy mount. The samples were ground and polished from both sides to a final thickness of approximately 40 μm. Thin films were also microtomed from both types of sample prior to, and following, the DMTA test. Specimens were examined in transmitted light with crossed polars in a Leitz optical microscope. High-magnification images utilized a high numerical aperture oil-immersion lens which allowed for the detection of birefringent objects at the limit of resolution.

Thin films were prepared for examination in a transmission electron microscope (TEM) to characterize the lamellar morphology of the different DMTA samples. The films were cast from a solution of 0.25 wt % sPS in xylene. Drops of the solution were placed on the surface of phosphoric acid held at $\sim 285\,^{\circ}C$. After the solvent evaporated the remaining thin film was quenched on to the surface of ice–water to prevent crystallization. The films were then washed, cut to the correct size and the thinnest portions were picked off the surface of a water bath using 1000 mesh TEM grids.

The solution-cast films were heat treated to simulate the thermal histories of the bulk samples. The small mesh size of the TEM grids were essential to support the film during the following procedure. To duplicate the lamellar structure of the slowly cooled plaques, the thin films were first melted at $340\,^{\circ}C$ and then cooled slowly at $10\,^{\circ}C\,min^{-1}$ to room temperature. The lamellar morphology of samples crystallized at low temperatures was produced by heating the quenched thin films at $5\,^{\circ}C\,min^{-1}$ from room temperature to either $142\,^{\circ}C$ or $155\,^{\circ}C$. The samples were rapidly cooled at $200\,^{\circ}C\,min^{-1}$ to room temperature from the maximum annealing temperature. The higher temperature coincided with the completion of primary crystallization at this heating rate.

The thin films were examined directly in the TEM without any additional treatment. A Jeol 100 transmission electron microscope was used at an acceleration voltage of 80 kV. All samples were viewed in bright-field mode with the images slightly defocused to increase contrast.

3. Results and discussion

3.1. Quenched sample micromorphology

For the bulk specimens, the rapid cooling by immersion in a liquid bath results in heat flow from the surface of the specimen. The rate of cooling, therefore, decreases with distance from the outer surface. Optical micrographs of transmitted light images taken with crossed polars reveal a core of strongly birefringent contrast (similar to small spherulites), and a surface region with no birefringent contrast. There is a relatively sharp boundary between the two regions at a distance, d, from the surface in the narrow range $340 < d < 390$ μm. Crystallinities are measured using fast scans in the DSC, and typically 3% crystallinity was measured in the surface region, and 48% in the core. The latter amounts are similar to those found in slowly cooled samples.

The DMTA tests involve the annealing of the specimen by heating the sample at a linear rate (with respect to time) up to a maximum temperature of $250\,^{\circ}C$ (below the melting point). The crystallinity of the specimens after the DMTA scan increases in all cases: the initially slowly cooled samples to 55%, and the initially quenched sample to 52%.

3.2. Estimating the mechanical properties of the quenched region

The variation in morphology across the quenched bar section, and the relatively sharp boundary delineating the largely amorphous surface regions from the crystalline core, suggest that these samples are essentially mechanically composite beams. The layered macrostructure consists of a crystalline core and the amorphous outer layers. To obtain an accurate estimate of the modulus of the initially amorphous region in the bending mode of the dynamic mechanical test, the measured geometry of the layered structure is used in a simple three-layer beam model. The modulus of

the outer layers, E'_o, is given by:

$$E'_o = \frac{E'_{co}(t^3) - E'_{in}(h^3)}{(t^3 - h^3)} \quad (1)$$

where E'_{co} and E'_{in} are the measured modulus of the entire beam and the crystalline core, h is the thickness of the inner core, and t is the thickness of the whole bar.

3.3. Changes in modulus resulting from crystallization

During the dynamic mechanical tests the temperature increases from 50 °C to 250 °C. For all the samples there is a large decrease in the storage modulus at approximately 100 °C (Fig. 1), which corresponds to the glass transition temperature of the atactic form of polystyrene [16]. The magnitude of this change varies from sample to sample, and this is discussed below. The increase in modulus of sample RC immediately following T_g is caused by crystallization of the metastable quenched amorphous material (Fig. 2). The same heating rate is used for both the DSC (crystallinity measurements) and the DMTA (modulus measurements. Crystallization and the change in the modulus occur over approximately the same temperature range $130 < T < 155$ °C. The measured crystallinity at $T = 150$ °C is $x_c = 48\%$.

As the samples are heated above this temperature, both the initially amorphous (RC) and melt crystallized (SC) show slight increases in crystallinity, and at the completion of the DMTA runs, both SC and RC samples have $x_c \cong 53\%$. Fig. 2 also shows, as expected for the melt-crystallized material (SC), no crystallization exotherm near 140 °C. However, it does show a double crystalline melting peak near 275 °C. The high temperature peak is the result of melting and recrystallization during the heating scan [11]. The lamella which first melt at low temperatures subsequently recrystallize due to the high degree of undercooling. These recrystallized lamella then melt, resulting in an additional peak in the melting endotherm.

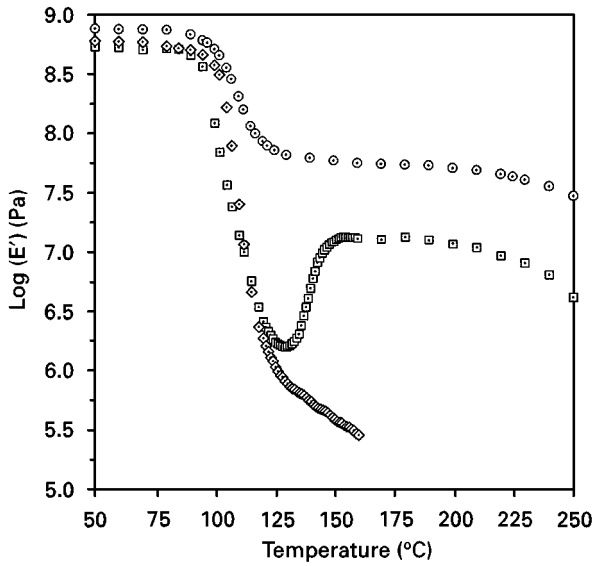

Figure 1 The storage modulus of (⊙) the slowly cooled bar (sample SC), (⊡) the quenched bar (sample RC), and (◇) atactic polystyrene.

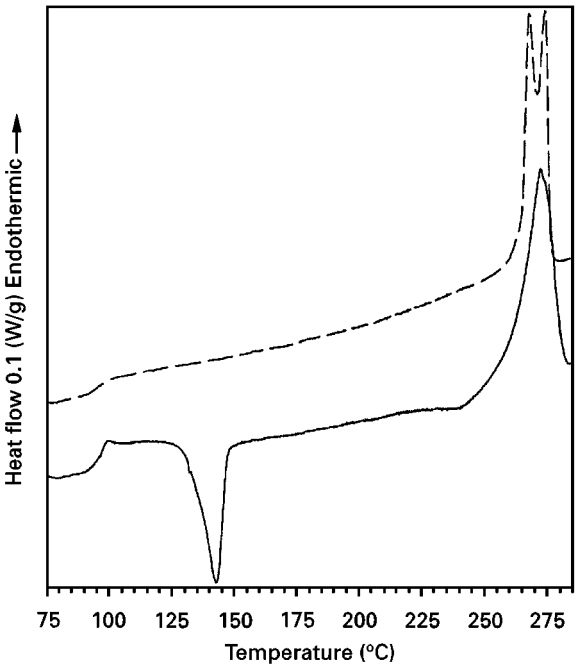

Figure 2 DSC thermograms at 5 °C min^{-1} of (—) sample RC and (– – –) sample SC.

Surprisingly, although these samples with different thermal history (RC and SC) have a similar crystalline content for temperature above ~150 °C, their storage moduli are very different, the sample SC being about an order of magnitude larger (Fig. 1). In this same temperature range, the modulus of the crystalline samples is much larger than that of the atactic sample, which is expected, because the crystalline phase is not expected to soften as much as the temperature increases through T_g.

In the two-phase crystalline–amorphous composite, the softening which occurs on heating near $T = 100$ °C may occur in either or both phases. The relative contributions to the decrease in modulus associated with each phase can be estimated by measuring the change in loss tangent peak magnitude with changes in crystallinity [17, 18] (Fig. 3). For comparison, the purely amorphous atactic polystyrene peak is seen here to have a peak value (tanδ-2) which is similar to the amorphous sPS peak reported in the literature [5]. As the initial crystallinity increases, the maximum loss tangent decreases. Extrapolation to a fully crystalline sample ($x_c = 1$) shows that the relaxation occurs almost entirely within the amorphous phase and mechanically the crystalline phase does not soften as the temperature increases through T_g. However, the difference between the two crystalline (sPS) samples above the amorphous glass transition temperature is notable, especially because the crystallinities are approximately the same. The mechanical properties of sPS are thus strongly dependent upon not only on the amount of crystalline phase, but on some other morphological-dependent effect which arises from the different thermal histories. The microstructural origin of this difference can be studied by examining the

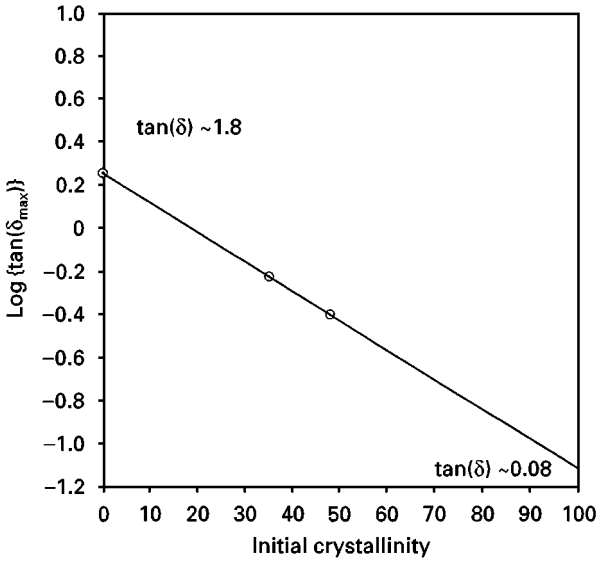

Figure 3 Peak values of tanδ for (⊙) samples of different initial crystallinity. The data for the 0% crystalline content sample are from atactic polystyrene.

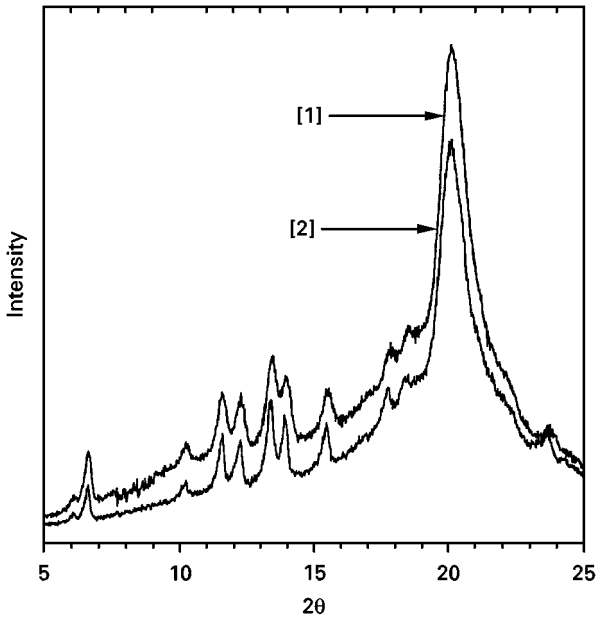

Figure 4 X-ray diffraction patterns of sample SC; (1) prior to, and (2) following the DMTA test.

micromechanical behaviour of this material, taking into consideration its two-phase composite microstructure.

Mechanically, a semi-crystalline polymer is a composite formed of crystalline and amorphous phases [19]. In macroscopic composites, bulk properties are averages of the properties of the constituent regions, with variations due to the size, shape and distribution of the phases. For sPS, several different crystal structures are found depending on the thermal history of the specimen, and some are expected to have different moduli.

3.4. Thermal history-dependent crystal structures

There is a difference in the crystal forms found in the slowly cooled and the quenched–annealed samples. For sPS, both the type and the quantity of the crystal form depends on the processing conditions [11, 20]. In the present study, the crystal structure of each sample was identified by indexing the diffraction pattern [1, 18, 20–23].

The X-ray diffraction patterns for sample SC, which was slowly cooled from the melt, are shown in Fig. 4. For this type of sample there is no change in the type of crystal form(s) present as a result of annealing which occurs during the DMTA test. The two polymorphs found in this sample have a planar zigzag conformation and differ only in the mode of packing [23]. The appearance of peaks at $2\theta = 10.3^\circ$, 14° and 15.5° indicates the α-form is of the more ordered modification [11]. In addition, the peaks at $2\theta = 6.03^\circ$, 12.3° and 18.6° indicate the presence of the β-form. The amount of each form was estimated from the intensity of the peaks at 11.6° and 12.4° [11, 22]. Sample SC is approximately 70% α-form and 30% β-form.

The X-ray diffraction patterns for rapidly cooled sample RC are shown in Fig. 5. The two broad peaks

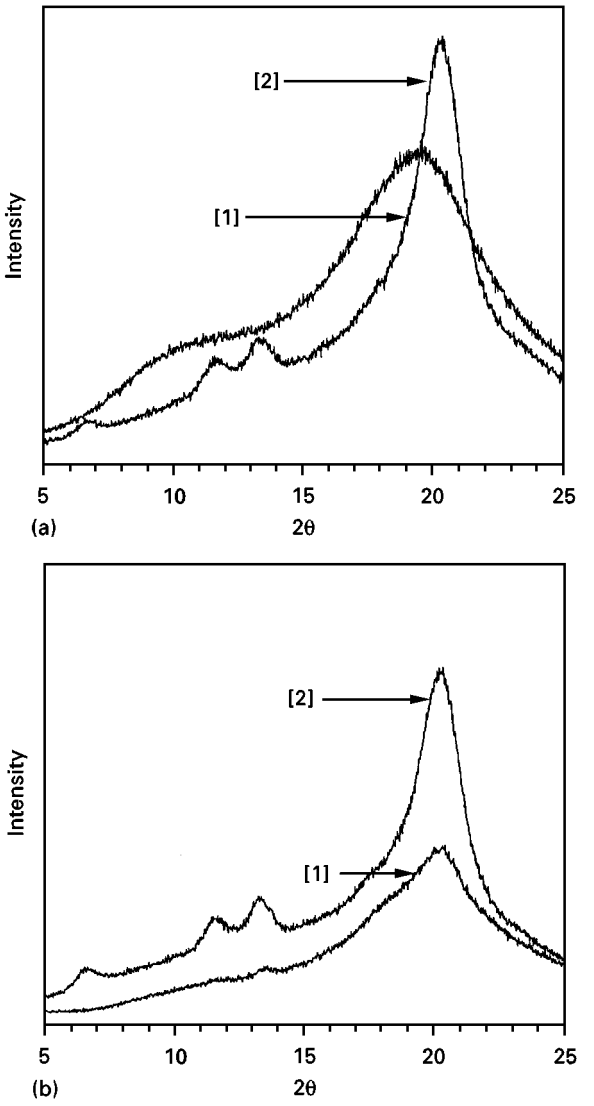

Figure 5 X-ray diffraction patterns of sample RC at (a) the outer surface, and (b) 400 μm from the outer surface. At both depths, the diffractions patterns were recorded (1) prior to and (2) following the DMTA test.

centred at about $2\theta = 9^\circ$ and 20° in Fig. 5a show that prior to the dynamic mechanical test the outer surface of a quenched sample is amorphous. The diffraction pattern of amorphous sPS is similar to that of atactic polystyrene [21]. The absence of certain peaks that are characteristic of the more ordered modification indicates that after the DMTA scan the crystal structure is of the less ordered α' modification. The crystal form present in this sample agrees with the observation of Guerra *et al.* [11] and DeRosa *et al.* [19], who found that the formation of the α' form is favoured during a quench from the melt or during crystallization at a temperatures close to T_g.

For sample RC, X-ray diffraction patterns at a depth of 400 μm from the other surface are shown in Fig. 5b. The very low intensity of all the peaks indicates that there is a low crystallinity at this depth prior to the DMTA test. After the test there is an increase in both the number of peaks and in their intensity. The peaks are however, broad compared to a slowly cooled samples which indicates a lower degree of crystal perfection is obtained. Peaks that are characteristic of the more ordered α' modification are absent, which shows that both the core and the outer layer are of the α'-form after the DMTA test. Both the α' and α'' modifications have a hexagonal crystal structure [18]. These modifications differ only in the arrangement of the main chain atoms. In the former there is a statistical disorder in the orientation of these chains but the benzene rings have the same positions as in the more ordered modification [11].

Differences in the conformation and in the packing arrangement of the chains in polymer crystals can, in some cases, affect the modulus. In crystalline forms of polystyrene, significant differences in modulus are predicted only for large differences in crystal structure. In particular the packing conformation is reported to be important helical being much softer than the planar zigzag arrangement [5, 16, 24]. Only the α and β forms (both have planar zigzag conformations) are found in the variously heat-treated samples, although the sample SC has a much as 30% β. The moduli for these two polymorphs are essentially identical [25] and differences in proportions found after different thermal histories are not expected to affect the composite properties.

3.5. Morphological effects on composite modulus

The differences in modulus observed between the samples SC and RC are, therefore, not due to differences in crystal structure, but rather due to differences in morphology of the crystalline and amorphous phases. Transmission electron micrographs show the distinctive lamellar structures for the sPS crystallized by slow cooling from the melt (SC) and by heating the quenched amorphous material (RC) (Figs 6 and 7).

For the two-phase (crystalline–amorphous) microstructures, the expected composite modulus can be calculated for varying crystallinity samples using the simple Voigt and Reuss averages which define the upper and lower bounds [26–28]

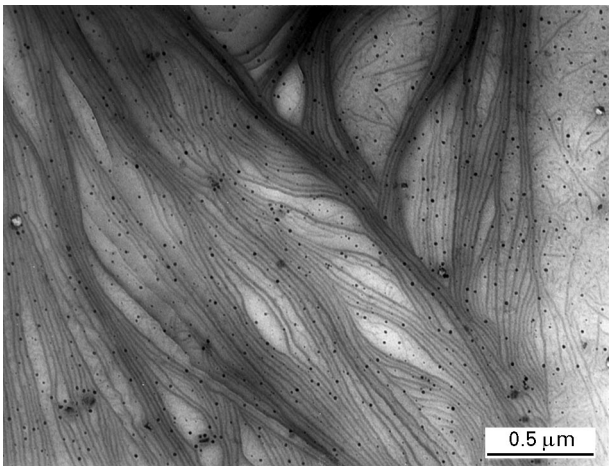

Figure 6 Transmission electron micrograph showing the lamellar morphology of a melt-crystallized sample.

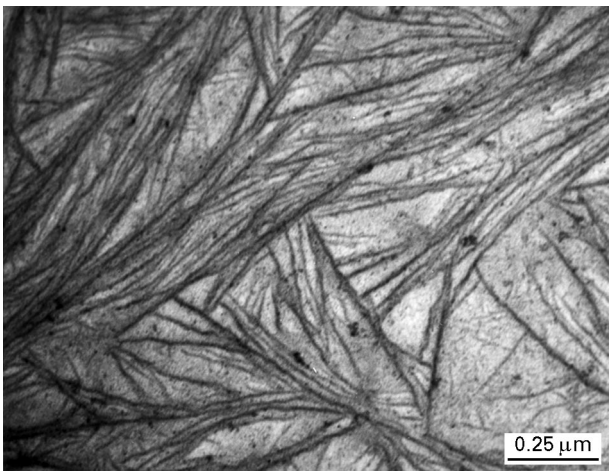

Figure 7 Transmission electron micrograph of lamellae in an initially amorphous thin film crystallized by heating at $5\,^\circ C\,min^{-1}$ from room temperature to 155 °C.

$$E'_{co} = (1 - x_c)E'_a + x_c E'_c \quad (2)$$

$$\frac{1}{E'_{co}} = \frac{(1 - x_c)}{E'_a} + \frac{x_c}{E'_c} \quad (3)$$

where E'_a is the modulus of the amorphous component, E'_c is the modulus of the crystalline component, and x_c is the crystalline content. Using Equations 1 and 2 and the experimental data shown in Fig. 3, the modulus of the crystalline phase is found to be 1.0×10^9 Pa at temperature below T_g. This estimate of E'_c does not consider the anisotropic character of the lamellae. At higher temperatures ($T > T_g$), the crystalline fraction does not soften appreciably and the upper and lower bounds for the modulus of the composite (crystalline + amorphous) can be calculated from Equation 2 and 3 (Fig. 8).

With heating, the crystallinity of sample RC increases from an initial value of ~3% to a value of 48% at 150 °C. For sample SC the crystallinity increases from an initial value of 48% to a final value of 55%. For this sample, the upper and the lower bounds

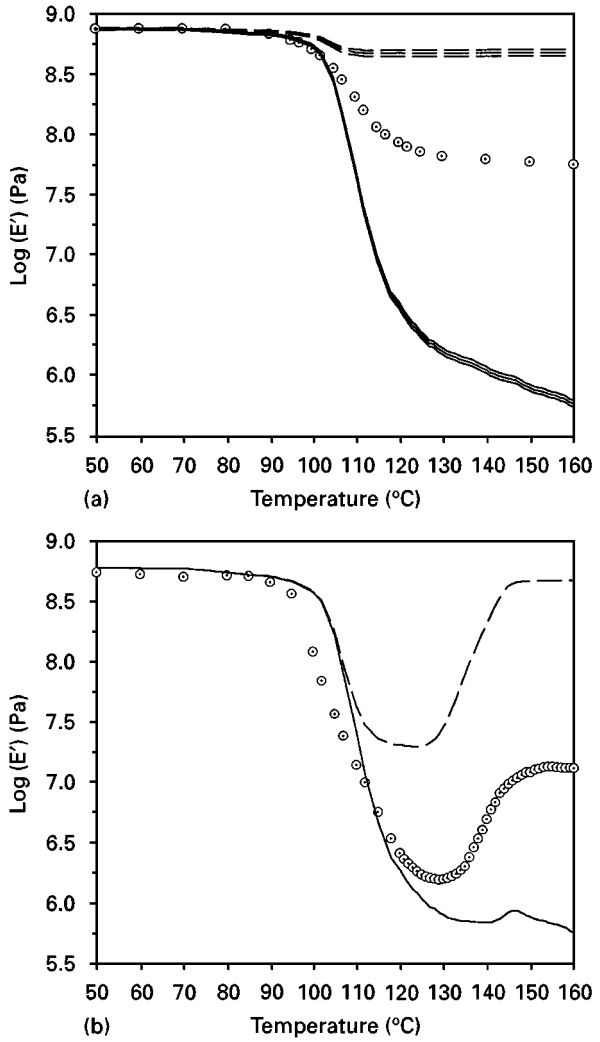

Figure 8 (– – –) Upper bound and (—) lower bound for (a) sample SC, and (b) sample RC. (⊙). The storage modulus of the sPS sample. In (a) the upper and lower bounds were calculated using three different values for x_c (48%, 51% and 55%).

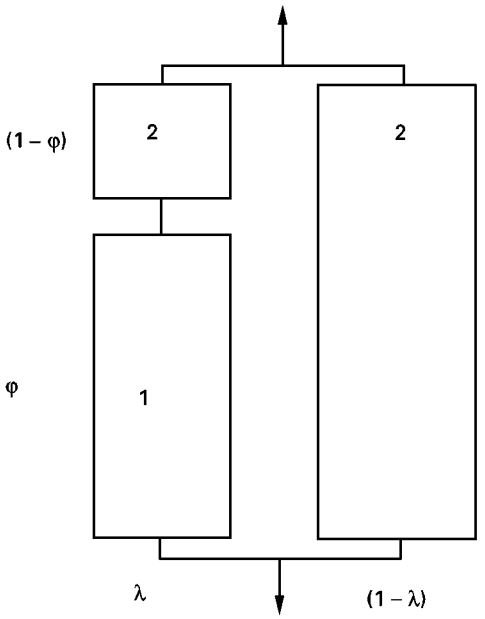

Figure 9 Parallel-series Takayanagi model for a two-phase polymer. Component 1 is dispersed in a matrix of component 2. The volume fraction of phase 1 is given by the product of the mixing parameters φ and λ.

were both calculated in the range $48\% < x_c < 55\%$ and are seen to be insensitive to these minor changes in the initial crystalline content. These simple parallel and series coupled models clearly predict composite moduli which are very different from the experimental values. A possible source of these discrepancies may be found by examining the contiguity of the phases. For composite materials, consisting of two or more mechanically distinct phases, the average properties are strongly dependent on which of the phases is contiguous, i.e. which phase acts as the matrix material.

Takayanagi and co-workers [24, 29, 30] developed micromechanical models which address this problem. These are two component models originally developed to describe the behaviour of multiphase polymers. Rather than use either a simple series or parallel coupled model, mixtures of the two are used. The arrangement of the individual components in the parallel–series model is shown in Fig. 9. In this combination, phase 1 is dispersed in a continuous phase 2. The terms φ and λ are parameters which are related to the mixing state and the phase proportions. The modulus of this system is given by [29]

$$E'_{co} = \lambda\left[\frac{\varphi}{E'_1} + \frac{(1-\varphi)}{E'_2}\right]^{-1} + (1-\lambda)E'_2 \qquad (4)$$

The product $\varphi\lambda = x_1$ is the volume fraction of the dispersed phase, which is determined from the experimental measurement of crystallinity at each temperature. If the crystallites are dispersed in a contiguous amorphous matrix, $\varphi\lambda = x_c$. If the role of the two phases is reversed the crystalline phase is contiguous and $\varphi\lambda = (1 - x_c)$.

Early applications of this model in partially crystalline polymers (high-density polyethylene) assumed the amorphous phase to be dispersed in a crystalline matrix [30]. The converse, in which the amorphous phase is contiguous, has also been used in other cases [31, 32]. Although some useful qualitative properties of the micromechanical model can be predicted (for example, in terms of contiguity of phases) from this model, its principal value in the present experiments is to examine the evolution of the modulus with crystallization in parametric terms. Normally the quantitative comparison of moduli from different specimens is difficult to make accurately, because of the variation in specimens and test parameters. In the present experiments, the nature of the experiment lends itself to an accurate comparison because the modulus is observed to change with increasing temperature in a single specimen (Fig. 1). The changes in modulus in one particular experiment, therefore, are not dependent on the specimen-to-specimen variability, nor on the differences in geometry of the test bar. In a simple curve-fitting model such as the Reuss and Voigt averages, or the one proposed by Takayanagi, if the model predicts the modulus at one temperature, it might be

expected to fit over the entire temperature range with appropriate changes in the volume fractions.

Applying Equation 4 to the material slowly cooled from the melt (SC), variations in φ result in large changes in the composite modulus for both possibilities: contiguous amorphous and contiguous crystalline. However, if matched at low temperature, the slopes of the $\log E'$ versus T predicted curves cannot be fitted to the experimental data and at high temperatures there is a large discrepancy, particularly with a contiguous amorphous component (Fig. 10). The agreement is better above T_g if the crystalline phase is contiguous but the model still does not predict the gradual decrease in the sample's modulus (Fig. 11). Similarly, the rapidly cooled sample (RC), which crystallizes above T_g, can be fitted only over limited ranges of temperature (Fig. 12). For sample RC, there is a discrepancy between the model and the experimental modulus between 90 and 105 °C. Quenched sPS has a broader dispersion than atactic polystyrene (Fig. 1) and, as a result, the model predicts a narrower relaxation. The wider dispersion may be due to the small initial crystalline fraction in sample RC. The predicted modulus also does not agree with sample RC at temperatures above 140 °C (Fig. 12).

There are two simple methods to improve the fit of the model to the data. The first is to assume the parameters λ and φ change with temperature (and crystallization). For sample SC there is, however, no evidence to suggest that these parameters change over the temperature range considered ($T < 160$ °C): the crystalline content increases only slightly during the DMTA test and the lamellar morphology remains unchanged. The second method to obtain a better fit is to assume the effective modulus of the amorphous phase increases with crystallization. There is evidence that this is a reasonable hypothesis. The relative amounts of the phases, and the micromorphology do not change significantly once the major crystallinity has developed (by 150 °C). Hence the Takayanagi parameters, which reflect the nature of the average coupling between the phases, are not expected to vary significantly at these temperatures. The relative direction of this deviation (the predicted modulus is less than the experimental), can arise if the amorphous phase has a stiffness higher than expected.

A physical rationale for this can be found by considering the crystalline–amorphous composite to be similar micromechanically to a steel–rubber layered composite structure. As the thickness to width ratio of the incompressible rubber layer decreases, the rubber effectively becomes stiffer perpendicular to the plane

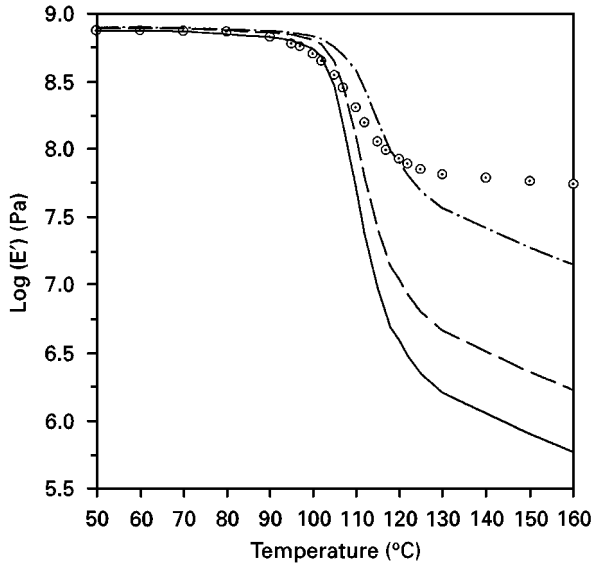

Figure 10 (⊙) Storage modulus of sample SC. The modulus calculated using the Takayanagi model with a contiguous amorphous phase is shown for (—) φ = 0.55, (– – –) φ = 0.90, and (–·–) φ = 0.99. Above T_g, the model describes the experimental data poorly, regardless of the value φ.

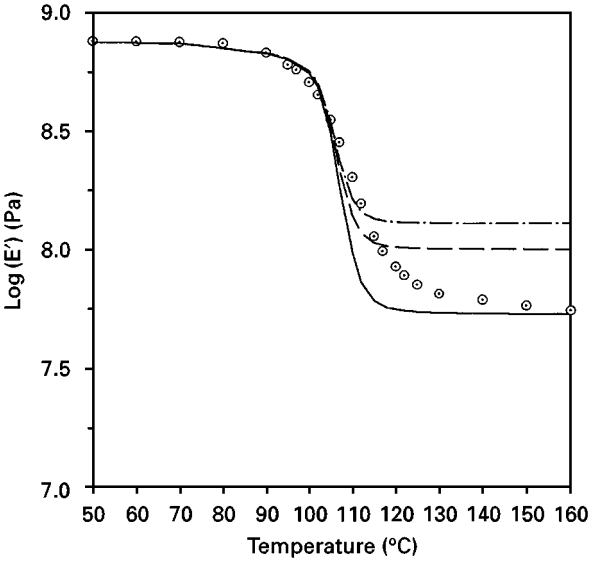

Figure 11 (⊙) Storage modulus of sample SC. The modulus calculated using the Takayanagi model with a contiguous amorphous phase is shown for (—) φ = 0.52, (– – –) φ = 0.55, and (–·–) φ = 0.60. Above T_g, the best fit is found for φ = 0.52.

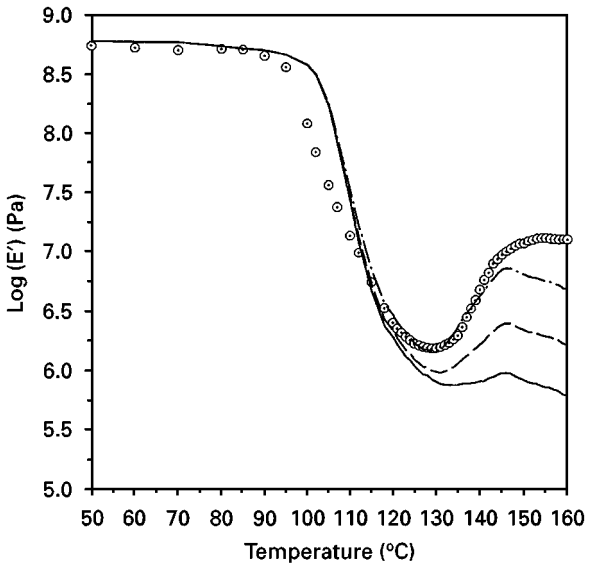

Figure 12 (⊙) Storage modulus of sample RC. The modulus calculated using the Takayanagi model with a contiguous amorphous phase is shown for (—) φ = 0.60, (– – –) φ = 0.90, and (–·–) φ = 0.97 (the best fit).

of the layer because of the constraint imposed on the softer phase by the stiffer phase. The conditions are found in sPS as the temperature increases ($T > T_g$), where the crystalline modulus remains high and the amorphous phase softens considerably. This macroscopic concept has previously been applied by Arridge and co-workers to the microscopic constraint of amorphous interlamellar regions in partially crystalline polymers such as polyethylene and in lamellar microstructures in oriented block copolymers [18, 33–36].

The geometry of the model is shown in Fig. 13. The subscript c refers to the crystalline lamellae and the subscript a to the interlamellar amorphous layer. Each layer is of thickness t_i (where i = a or c) width w and length L. In this figure, L is parallel to the z-axis. If the applied stress is perpendicular to the x–z plane then the stress in each layer may be considered two-dimensional if the lamellae are very much longer in the growth direction than in the lateral dimensions. For lamellae in spherulites this assumption is usually correct because L is much larger than the maximum lateral dimension, w [34]. Although applied to multilayer structures such as oriented crystalline or block copolymers, the constraint argument will hold for any thin rubbery layer constrained between stiffer plates. The constraint effect is observed for tensile stresses applied perpendicular to the plane of the rubbery layer, and is not seen for tensile stresses in the plane of the layer. In spherulitic polymers, only a fraction of the lamellae are oriented to produce maximum constraint, and there is a progressive decrease in constraint as the interlamellar plane rotates away from the perpendicular orientation [33]. In the Takayanagi model fit for the present experiments a fraction of the amorphous material is oriented with respect to the applied stress as shown in Fig. 13 and will therefore be constrained. The constriant effect is also critically dependent on the relative moduli of the two phases. Below T_g the crystalline and amorphous phases have similar moduli which diverge drastically as the temperature increases above T_g, the amorphous phase becoming approximately two orders of magnitude smaller, which is similar to the difference used in earlier constraint models on partially crystalline polymers [36].

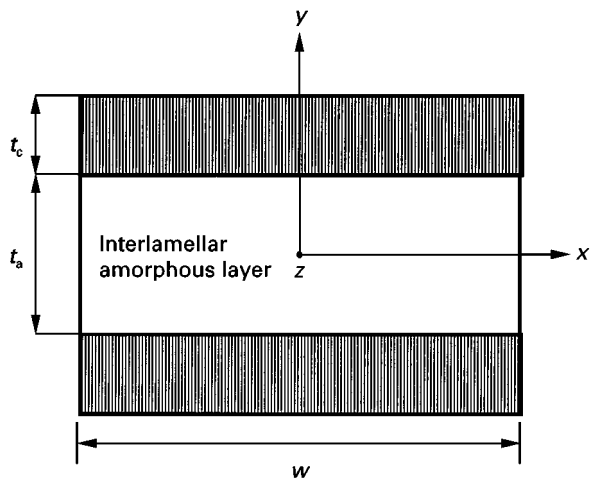

Figure 13 Definition of axes for an oriented lamellar stack.

The micromorphology of the lamellae in the present study is consistent with this kind of constraint model. The interlamellar spacing of the SC (melt crystallized) sPS is about 11 nm (Fig. 6). The visible lateral extent of the lamellae is greater than 1 μm, giving an aspect ratio of approximately 0.01 (thickness to length) for the rubbery interlayer. For the rapidly cooled samples, the interlamellar spacing is larger (30 nm) and the maximum dimension of the lamellae is smaller, approximately 1 μm (Fig. 7). The aspect ratio of the interlamellar layers is therefore larger and as a result the amorphous material is less constrained.

For the SC sample the increase in the composite modulus due to the constraint of the amorphous material can be estimated by modifying the modulus of this component by a factor k. Equation 4 now becomes

$$E'_{co} = \lambda\left[\frac{\varphi}{E'_1 k} + \frac{(1-\varphi)}{E'_2}\right]^{-1} + (1-\lambda)E'_2 \qquad (5)$$

where phase 1 is the dispersed amorphous component. The value of the parameters φ and λ have been determined from the previous analysis and the best fit was found for $\varphi = 0.52$. The modulus of the SC sample can now be modelled with a temperature-dependent k (Fig. 14a).

Over the range of temperatures $90 < T < 160\,^{\circ}C$, the minor increases in crystallinity or changes in lamellar morphology, are completed for the initially slowly cooled sample (SC). Starting a low T, $k = 1$, and no constraint effect is present because the amorphous phase is glassy [34]. The amorphous and crystalline phases have similar elastic properties, with Poisson's ratio $\nu \sim 0.35$ [37] and modulus $\sim 10^{8.8}$ Pa. As the temperature increases, the constraint effect is expected to become significant for $T > T_g$, as the amorphous phase becomes softer and approximately incompressible [36]. The change in the modulus of the amorphous component is shown in Fig. 1 by the atactic storage modulus, which becomes approximately two orders of magnitude softer than the glassy state as the temperature increases to $T = 115\,^{\circ}C$. At this temperature, the amorphous phase is soft enough relative to the lamellae that the constraint effect is fully effective ($k = 10$ in Fig. 14b). Between 100 and 120 °C, k increases by a factor of 10. Above this upper temperature, k and, therefore, the constraint effect, remain constant.

For the sPS which is initially quenched (sample RC), the increase in crystallinity above T_g occurs simultaneously to the increase in amorphous phase constraint (Fig. 14a). The modulus of the amorphous phase in the series configuration is estimated by adjusting the curve fit with variations in k. The modulus of the constrained interlamellar material in this case if $E'_2 k$, because unline the sample SC, for the sample RC the amorphous phase is contiguous. Below 130 °C this sample has a small crystalline fraction and the constraint effect is negligible. The constraint of the amorphous material begins to affect the composite

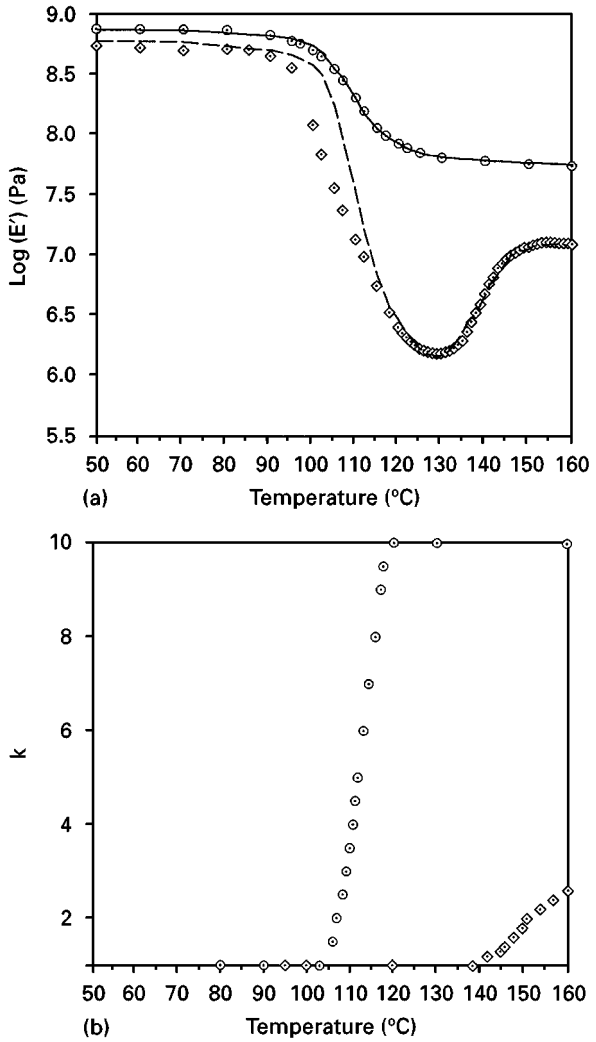

Figure 14 (a) Modulus of samples (⊙) SC and (◇) RC. For both, the modulus is calculated using the Takayanagi model with the best fit value for φ from the previous analysis; (—) sample SC, (– – –) sample RC. Above T_g, the amorphous phase is constrained with its modulus increased by a factor k. The change in k with temperature is shown in (b) for (⊙) sample SC, and (◇) sample RC.

mechanical properties only as the temperature increases above approximately 140 °C (Fig. 14b). Between this temperature and 160 °C, the constraint factor, k, increases from 1 to $\sim$2.5 and the crystallinity approximately doubles. The interlamellar layers are thus constrained only at high temperature where the amorphous phase is soft, and in microstructures in which there is sufficient constraining crystalline phase ($x_c > 25\%$).

As crystallization proceeds in the sample RC at even higher temperatures, the aspect ratio of the interlamellar material decreases (thickness to lateral dimension) and the constraint effect becomes more pronounced. This can be qualitatively confirmed by comparing the transmission electron micrographs for two samples which are both initially quenched to the amorphous state: the first is heated to 142 °C (Fig. 15) and the second is heated to 155 °C (Fig. 7), and the progressive crystallization can be observed clearly. The initial stages of solid-state crystallization result in a small number of relatively widely spaced lamellae

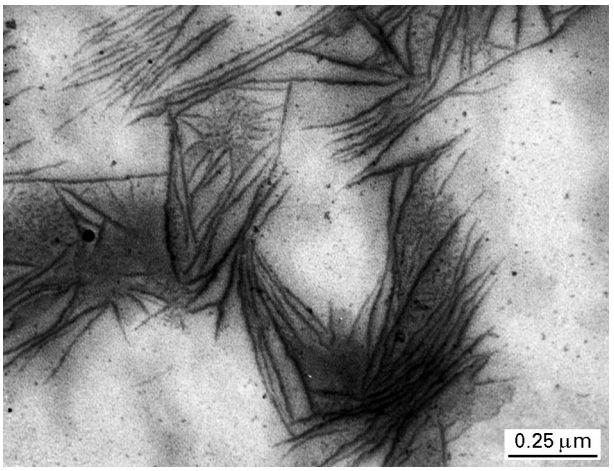

Figure 15 Transmission electron micrograph of lamellae in an initially amorphous thin film crystallized by heating at 5 °C min^{-1} from room temperature to 142 °C.

(the interlamellar regions have a large aspect ratio), while the later stages result in more closely spaced and longer lamellae (the interlamellar regions have a much smaller aspect ratio).

4. Conclusion

The crystallization history of sPS affects its mechanical properties. As expected, larger amounts of the stiffer crystalline phase result in higher moduli. However, samples cooled slowly from the melt are much stiffer than are samples quenched from the melt (to the amorphous state) and subsequently heated to induce crystallization just above T_g. This is found for specimens with nominally the same crystalline content. The experimental measurements follow single specimens which progressively crystallize on heating, and measured change in modulus are clearly not ascribable simply to changes in crystallinity. Examination of the lamellar structure and micromechanical modelling of the two different micromorphologies which evolve show that the most likely reasons for these differences are the constraint of the amorphous phase by the high-modulus lamellae, and the variation in phase contiguity. In slowly cooled samples the crystalline phase is contiguous (mechanically), and the interlamellar amorphous material is more highly constrained than in quenched–annealed samples. The average mechanical properties of syndiotactic polystyrene can thus be strongly affected by the micromorphology, which is, in turn, controlled by its thermal history.

References

1. N. ISHIHARA, T. SEIMIYA, M. KURAMOTO and M. UOI, *Macromolecules* **19** (1986) 2465.
2. L. C. LOPEZ, R. C. CIESLINSKI, C. L. PUTZIG and R. D. WESSON, *Polymer* **36** (1995) 2331.
3. Y. ULCER, M. CAKMAK, J. MIAO and C. M. HSIUNG, *J. Appl. Polym. Sci.* **60** (1996) 669.
4. S. WU, R. A. BUBECK and C. J. CARRIERE, *ibid.* **62** (1996) 1483.

5. F. De CANDIA, R. RUSSO and V. VITTORIA, *J. Polym. Sci. C Polym. Lett*. **28** (1990) 47.
6. F. De CANDIA, G. ROMANO, R. RUSSO and V. VITTORIA, *Coll. Polym. Sci.* **268** (1990) 720.
7. V. VITTORIA, A. RUVOLO FILHO and F. De CANDIA, *J. Macromol. Sci. Phys.* **B29** (1990) 411.
8. E. J. C. KELLAR, C. GALIOTIS and E. H. ANDREWS, *Macromolecules* **29** (1996) 3515.
9. A. M. EVANS, E. J. C. KELLAR, J. KNOWLES, G. GALIOTIS, C. J. CARRIERE and E. H. ANDREWS, *Polym. Eng. Sci.* **37** (1997) 153.
10. S. ST. LAWRENCE and D. M. SHINOZAKI, *ibid*. **37** (1997) 1825.
11. G. GUERRA, V. VITAGLANAO, C. DE ROSA, V. PETRACCONE and P. CORRADINI, *Macromolecules* **23** (1990) 1539.
12. G. GUERRA, C. DE ROSA, V. VITAGLIANO, V. PETRACCONE and P. CORRADINI, *J. Polym. Sci. B Polym. Phys.* **29** (1991) 265.
13. D. H. KRZYSTOWCZYK, X. NIU, R. D. WESSON and J. R. COLLIER, *Polym. Bull.* **33** (1994) 109.
14. E. J. C. KELLAR, A. M. EVANS, J. KNOWLES, C. GALIOTIS and E. H. ANDREWS, *Macromolecules* **30** (1997) 2400.
15. A. J. PASZTOR, B. G. LANDES and P. J. KARJALA, *Thermochim Acta.* **177** (1991) 187.
16. N. G. McCRUM, B. E. READ and G. WILLIAMS, "Anelastic and Dielectric Effects in Polymer Solids" (Dover Publications, New York, 1967) p. 412.
17. R. W. GRAY and N. G. McCRUM, *J. Polym. Sci. A-2* **7** (1969) 1329.
18. O. GREIS, Y. XU, T. ASANO and J. PETERMANN, *Polymer* **30** (1989) 290.
19. R. G. C. ARRIDGE, "An Introduction to Polymer Mechanics" (Taylor and Francis, London, 1985).
20. C. DE ROSA, M. RAPACCIUOLO, G. GUERRA, V. PETRACCONE and P. CORRADINI, *Polymer* **33** (1992) 1423.
21. V. VITTORIA, R. RUSSO, F. De CANDIA, *J. Macromol. Sci. Phys.* **B28** (1989) 419.
22. V. VITTORIA, A. RUVOLO FILHO and F. De CANDIA, *ibid*. **B31** (1992) 133.
23. R. NAPOLITANO and B. PIROZZI, *Macromolecules* **26** (1993) 7225.
24. M. TAKAYANAGI, K. IMADA and T. KAJIYAMA, *J. Polym. Sci. C* **15** (1966) 263.
25. Z. SUN, R. J. MORGAN and D. N. LEWIS, *Polymer* **33** (1992) 660.
26. W. VOIGT, "Lehrbuch des Krystallphysik" (Teubner, Leipzig, 1928) p. 410.
27. A. REUSS, *Z. Angew. Math. Mech.* **9** (1929) 49.
28. R. HILL, *Proc. Phys. Soc. A* **65** (1952) 349.
29. M. TAKAYANAGI, H. HARIMA and Y. IWATA, *Mem. Fac. Eng. Kyushu Univ.* **23** (1963) 1.
30. M. TAKAYANAGI, K. IMADA and T. KAJIYAMA, *J. Polym. Sci. C* **5** (1963) 113.
31. T. THISTLETHWAITE, R. JAKEWAYS and I. M. WARD, *Polymer* **29** (1988) 61.
32. I. M. WARD, "An Introduction to the Mechanical Properties of Solid Polymers" (Wiley, New York, 1993) p. 157.
33. P. ALLAN, R. G. C. ARRIDGE, F. EHTAIATKAR and M. J. FOLKES, *J. Phys. D Appl. Phys.* **24** (1991) 1381.
34. R. G. C. ARRIDGE and M.W. B. LOCK, *ibid*. **9** (1976) 329.
35. R. G. C. ARRIDGE, *ibid*. **8** (1975) 34.
36. R. G. C. ARRIDGE, in "Polymer Blends and Alloys", edited by M. J. Folkes and P. S. Hope (Blackie Academic and Professional, London, 1993) p. 130.
37. M. A. JONES, C. J. CARRIERE, M. T. DINEEN and K. M. BOLWINSKI, *J. Appl. Polym. Sci.* **64** (1997) 673.

Received 27 November 1997
and accepted 15 May 1998